Final version published as: Eric M. Schibli, Andrew G. Wright, Steven Holdcroft, and Barbara J. Frisken. Morphology of Anion-Conducting Ionenes Investigated by X-ray Scattering and Simulation *The Journal of Physical Chemistry B* 2018 122 (5), 1730-1737. DOI: 10.1021/acs.jpcb.7b10177

Morphology of Anion-Conducting Ionenes Investigated by X-ray Scattering and Simulation

Eric M. Schibli,[†] Andrew G. Wright,[‡] Steven Holdcroft,[‡] and Barbara J. Frisken[*,†]

[†]*Department of Physics, Simon Fraser University, Burnaby BC Canada V5A 1S6*

[‡]*Department of Chemistry, Simon Fraser University, Burnaby BC Canada V5A 1S6*

E-mail: frisken@sfu.ca

Abstract

We have studied the morphology of a novel series of benzimidazole-based ionenes, methylated poly(hexamethyl-*p*-terphenyl benzimidazolium) (HMT-PMBI), in halide form. Materials with anion-exchange capacities ranging from 0 – 2.5 mequiv/g were studied. X-ray scattering reveals three length scales in the materials: ion-polymer spacing (4 Å), polymer-polymer interchain spacing (6 Å), and an intrachain repeat distance (20 Å). No long-range structure is apparent above the monomer length, which is rare in ion-conducting polymer membranes. In preliminary molecular dynamics simulations, water molecules were observed forming chains between ions, even at a modest level of hydration, providing an inter-penetrating network where conductivity can occur.

Introduction

Anion-exchange membranes (AEMs), formed from synthetic macromolecules containing fixed cationic sites and dissociated anions, are currently of considerable interest because of their importance in electrochemical technologies such as fuel cells, electrolysis,[1] wastewater treatment,[2] redox-flow batteries,[3] biofuel cells,[4] and desalination.[5] In particular, hydroxide-ion AEM fuel cells (AEMFC) and electrolyzers are energy converters of emerging interest because the use of non-precious metal catalysts in alkaline media offers an advantage over devices based on proton-exchange membranes.[6] However, challenges to widespread adoption of AEMs for these technologies include poor stability of polymeric materials in basic media[7] and comparatively poor ion conductivity due to the low diffusion coefficient of the hydroxide ion and its carbonation when exposed to air. The past five years have shown significant increases in reported AEMFC peak power and current densities; however, membrane stability remains a significant concern.[8] To address this concern, numerous cationic moieties have been investigated for hydroxide stability, including guanidinium,[9] DABCO,[10] imidazolium,[11] pyrrolidinium,[12] sulfonium,[13] phosphonium,[14] and ruthenium-based cations.[15]

This work focuses on a material that is based on a sterically-protected benzimidazolium-

based cation, methylated poly(hexamethyl-p-terphenyl benzimidazolium) (HMT-PMBI). This material has a tunable ion-exchange capacity and has been proven to possess ion conductivity and exceptional hydroxide stability.[16,17] HMT-PMBI has been demonstrated in both fuel cells and water electrolyzers.[17] In fuel-cell testing, HMT-PMBI cells exhibited exceptional stability leading to longer lifetimes. HMT-PMBI falls under a class of polymers known as ionenes for which the cation is an integral feature of the polymer backbone. In the case of HMT-PMBI, the stability of the cation is provided via steric protection by methyl groups;[18] however no investigations of the morphology or conduction mechanisms for HMT-PMBI or similar polymers have been reported to date.

An understanding of polymer morphology is an important component in the design of improved materials for polymer-electrolyte membranes.[19] Ion conduction involves the diffusion of ions through water-rich domains and depends both on charge content of the hydrophilic domains and on their interconnectivity. The morphology also impacts chemical and mechanical stabilities.

In this paper, we report a detailed analysis of the morphology of HMT-PMBI. We performed small- and wide-angle X-ray scattering (SAXS and WAXS) on two halide forms of HMT-PMBI, HMT-PMBI(I^-) and HMT-PMBI(Cl^-), in various conditions: in vacuum, in ambient conditions, after soaking in water, and after stretching. We also performed density functional theory calculations and preliminary molecular dynamics calculations to aid interpretation of our results.

Materials and methods

HMT-PMBI is a polymer composed of up to three submolecular units, x, y, and z, with each unit contributing either $+0$, $+1$, or $+2$ to the total charge of the backbone; the chemical structures are shown in Figs. 1 (a), (b), and (c), respectively. The cationic benzimidazolium units are separated by a series of neutral aromatic rings to reduce the material's solubility.

The ion-exchange capacity (charge content along the backbone) is determined by the relative ratio of x, y, and z units, which in turn is determined by the degree of methylation (dm).[16]

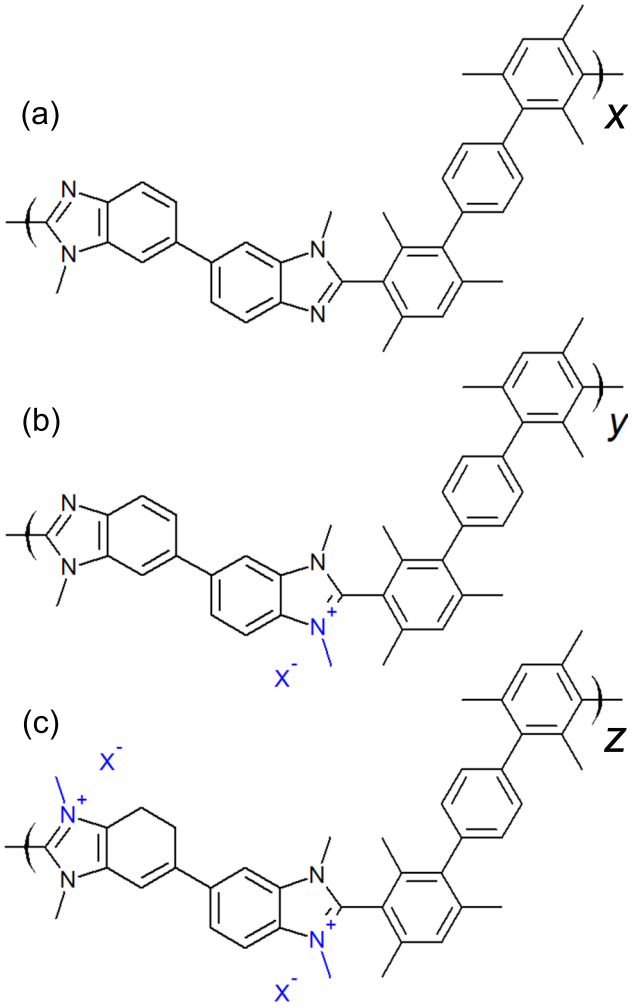

Figure 1: Chemical structure of HMT-PMBI, a polymer composed of three submolecular units: x, y, and z as shown in parts (a), (b), and (c) of this figure, respectively. The anion, X^-, is iodide immediately following synthesis.

The samples consisted of polymer films that were cast from dimethyl sulfoxide (DMSO) solutions formed by dissolving 0.20 g of polymer in 12 mL of hot DMSO. The resulting solutions were filtered into clean, flat Petri dishes and allowed to dry at 86 °C for 48 hr in air. The resulting transparent, brown films were removed by addition of water, which allowed films to be peeled off of the glass. They were then transferred into deionized water for at least 48 hours. The final films were approximately 50 μm thick. The films were cast in

iodide form. Some of the films were treated with potassium chloride or potassium hydroxide to exchange the iodide for chloride or hydroxide.

Samples resulting from casting of HMT-PMBI with four different degrees of methylation (dm) of the N sites of the submolecular units were investigated in this study. Samples were measured in the original iodide form, or after exchanging the iodide for chloride. The degree of methylation of the polymers ranged from 65.9 to 97.5% dm; a sample with a degree of methylation of 50%, is entirely uncharged and contains only (a) units. Table 1 reports values for: the degree of methylation, ion exchange capacity (IEC) for the dry membrane, water uptake, and ion conductivity.[16,17] The OH^- form of the polymer was air-equilibrated with the result that the anion was in mixed hydroxide-carbonate form. ^{1}H NMR spectroscopy was used to determine the degree of methylation, from which the IEC was calculated. For 97.5% and 80.7% dm HMT-PMBI in chloride and iodide form, hydrated weight was measured after soaking in de-ionized water for 16 hours at ambient temperature. Dry weight was measured after drying the samples for 24 hours at 353K in vacuum. The remaining material properties are reprinted from previous publications.[16,17]

Table 1: Properties of HMT-PMBI at varying degrees of methylation (dm)

dm (%)	anion[a]	IEC (mequiv/g)	water uptake (wt%)	σ[b] (mS/cm)
65.9	HCO_3^-/CO_3^{2-}	1.1	29 ± 4	0.10 ± 0.03
80.2	HCO_3^-/CO_3^{2-}	2.0	42 ± 3	1.4 ± 0.2
89.7	HCO_3^-/CO_3^{2-}	2.5	54 ± 2	10.0 ± 1.2
97.5	HCO_3^-/CO_3^{2-}	3.1	NA[c]	NA[c]
80.2	Cl^-	1.8	24 ± 8	NA[d]
89.7	Cl^-	2.5	37 ± 2	7.5 ± 0.4
97.5	Cl^-	3.0	90 ± 50	NA[d]
80.2	I^-	1.6	12 ± 4	NA[d]
89.7	I^-	2.5	16.0 ± 1.0	0.87 ± 0.01
97.7	I^-	2.3	17.3 ± 1.4	NA[d]

[a] The HCO_3^-/CO_3^{2-} form was obtained from exposure of the OH^- form to ambient atmosphere
[b] Ion conductivity
[c] Water-soluble material
[d] Not measured

X-ray scattering was performed using a SAXSLab Ganesha 300XL instrument located in 4D LABS at Simon Fraser University. The instrument includes a copper anode source operating at 50 kV and 0.6 mA, producing Kα radiation with a wavelength $\lambda = 1.54$ Å, and a mobile PILATUS3 R 300K photon counting detector. The entire instrument is housed in a 2 m vacuum chamber. Three scattering configurations – small-angle, medium-angle, and wide-angle X-ray scattering (SAXS, MAXS, and WAXS) – were achieved by moving the detector within the chamber, providing a usable q-range of 0.01 to 2.7 Å^{-1}, where $q = \frac{4\pi}{\lambda}\sin(\theta/2)$ is the scattering wave vector and θ is the scattering angle.

Samples were measured in vacuum, in ambient conditions, and after hydration. Samples measured in vacuum were affixed to a sample holder with double-sided tape and allowed to equilibrate within the evacuated instrument chamber for one hour. Samples measured in ambient conditions were placed inside a paste cell consisting of an O-ring spacer and mica windows, which isolated the sample from vacuum. Hydrated samples were submerged in water for one hour, following which excess water was removed from the films by dabbing with tissue paper before they were placed in a paste cell. The stretched sample was prepared by drawing a film at room temperature and ambient humidity until it broke at an extension ratio of approximately 2. Portions of the stretched sample from near the tear point were measured in vacuum.

A fitting function (Eq. S1) consisting of up to three pseudo-Voigt functions, a power law, and a q-independent background was fit to the data. The pseudo-Voigt function provides a flexible peak shape suitable for both crystalline and non-crystalline structure. The power law accounts for larger scale inhomogeneities in the sample. The measurement of wet 97.5% dm HMT-PMBI(Cl^-) showed a mid-q feature. This was fit to the Correlation Length Model (Eq. S2). Further details of analysis methods can be found in the Supporting Information. We assume that each visible peak corresponds to a single length scale in the material given by

$$d_i = 2.44 \times \frac{\pi}{q_i} \quad , \tag{1}$$

where q_i is the peak position, as recommended for scattering from amorphous polymers.[20]

Density functional theory (DFT) calculations were used to provide insight into the shape and electronic structure of the molecules. DFT calculations were performed using the Gaussian[21] quantum chemistry program, the B3LYP functional[22] and the def2-TZVP basis set.[23] Figure 2 shows the results of a geometry optimization of a cationic 100% dm HMT-PMBI tetramer at the B3LYP/def2-TZVP level of theory. Figure 2a shows the optimal nuclei positions; the molecule is highly extended, as it carries a net charge of +8 and is in vacuum. The methylated, neutral aromatic rings are rotated approximately 80° out-of-plane relative to their corresponding cationic benzimidazolium units. This orientation sterically protects the most vulnerable carbon atom, the C2 carbon, which is located at the apex of the benzimidazole unit. This is in general agreement with calculations and measurements performed on small molecule analogues[18] and is believed to greatly contribute to the stability of the hydroxide form of HMT-PMBI. In analysis of methylated *m*-PBI and ether-linked PBI, the C2 carbon was found to be vulnerable to hydroxide attack.[24] Figure 2c shows the molecular electrostatic potential along an electron density isosurface of 0.002 electrons/$a_0{}^3$, where a_0 is the Bohr radius. The highest potential is concentrated along the nitrogen-carbon-nitrogen "triangle" of the benzimidazole rings. The mesitylene-phenylene-mesitylene group maintains a low and approximately constant potential. This confirms that this section of the molecule is hydrophobic. As this oligomer has a net electric charge of +8, the potential of the entire surface is positive.

Molecular dynamics (MD) simulations were designed to aid interpretation of the WAXS results.[25,26] Preliminary MD simulations were performed using the GPU-accelerated distribution of NAMD 2.11[27,28] with OPLS-AA-based parameters;[29] details can be found in the Supporting Information. Parameters are listed in Tables S1, S2 and S3; OPLS-AA parameters as implemented in NAMD were used when available. CHarMM36 parameters[30] where used for dihedral angles involving nitrogen methyl groups as no OPLS-AA parameters were available. The DFT results provided the atomic partial charges and initial geometries for

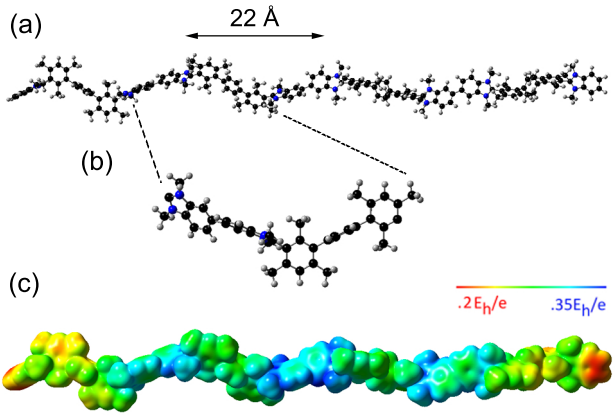

Figure 2: The results of the density functional theory calculation for fully methylated HMT-PMBI: (a) the optimized nuclei positions in a tetramer showing steric protection of the cationic region, (b) an expanded view of a single molecular unit, and (c) the electron density isosurface illustrating the relative hydrophilicity (blue) and hydrophobicity (green) of the molecule. The red areas are end effects due to the net positive charge of the molecule.

the tetramers in the MD simulations.

Results

X-ray scattering results for (a) HMT-PMBI(I^-) and (b) HMT-PMBI(Cl^-) samples of various dm in vacuum are shown in Fig. 3, plotted as a function of the magnitude of the scattering wave vector, q. Three peaks are visible in each measurement: a small, broad peak at approximately 0.4 $Å^{-1}$, and two WAXS peaks, at approximately 1.35 $Å^{-1}$ and 2.00 $Å^{-1}$. We refer to these peaks as Peak 0, Peak 1, and Peak 2, respectively; they correspond to length scales of approximately 20 Å, 6.4 Å, and 4 Å. Peak 2 increases in intensity with degree of methylation, while Peak 0 and Peak 1 show similar shape and intensity for different dm. Peak 2 is also much more clearly defined in the iodide form as compared to the chloride form of the polymer. The solid curves are fits of the model function to the data.

Figure 4 compares vacuum, ambient, and hydrated (wet) measurements for 80.2% and 97.5% dm HMT-PMBI in iodide and chloride form. All peaks shift to lower q with increased hydration, consistent with moderate swelling occurring during hydration. Peak 0 shrinks with increased hydration; it is no longer visible in the data for the wet chloride-form sam-

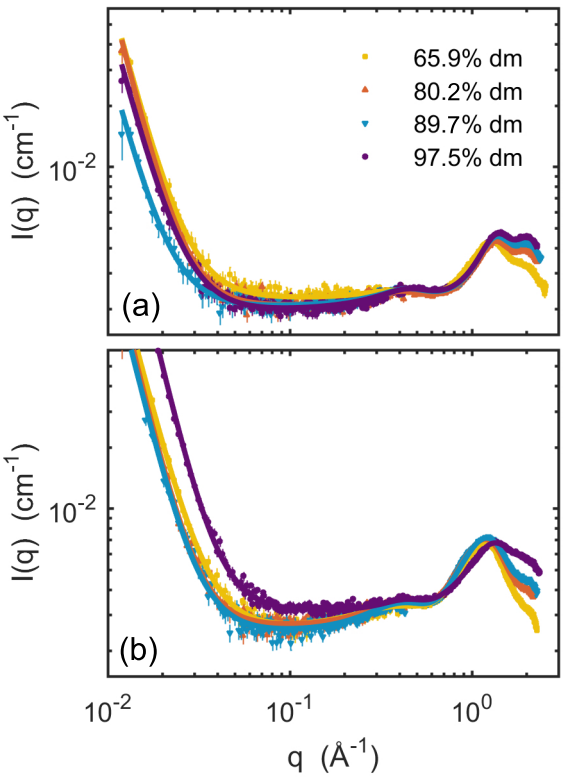

Figure 3: X-ray scattering profiles of films of (a) HMT-PMBI(I^-) and (b) HMT-PMBI(Cl^-) at degrees of methylation (dm) ranging from 65.9% to 97.5%, measured in vacuum. The solid curves are fits of Eq. S1 to the data.

ples. Except for the 80.2% dm HMT-PMBI(I^-) sample, which uptakes little water, Peak 2 increases in intensity with hydration. The measurement of hydrated 97.5% dm HMT-PMBI(Cl^-), which uptakes a very large amount of water, shows a mid-q shoulder.

Figure 5 compares scattering from a stretched and an unstretched sample. Figure 5 (a) shows the 2-D image of scattering from stretched 89.7% dm HMT-PMBI(I^-) as captured by the detector. The stretched sample produced an anisotropic scattering pattern. For this image, the sample was mounted with the stretching axis along the vertical axis. The larger diameter complete ring, which corresponds to Peak 1, shows stronger scattering in the direction perpendicular to the stretching axis, the equatorial direction. The smaller diameter partial ring, which corresponds to Peak 0, shows stronger scattering in the direction parallel to the stretching axis, the meridional direction. To achieve a good coverage of q-space, it was necessary to repeat the measurements after rotating the sample by 90°.

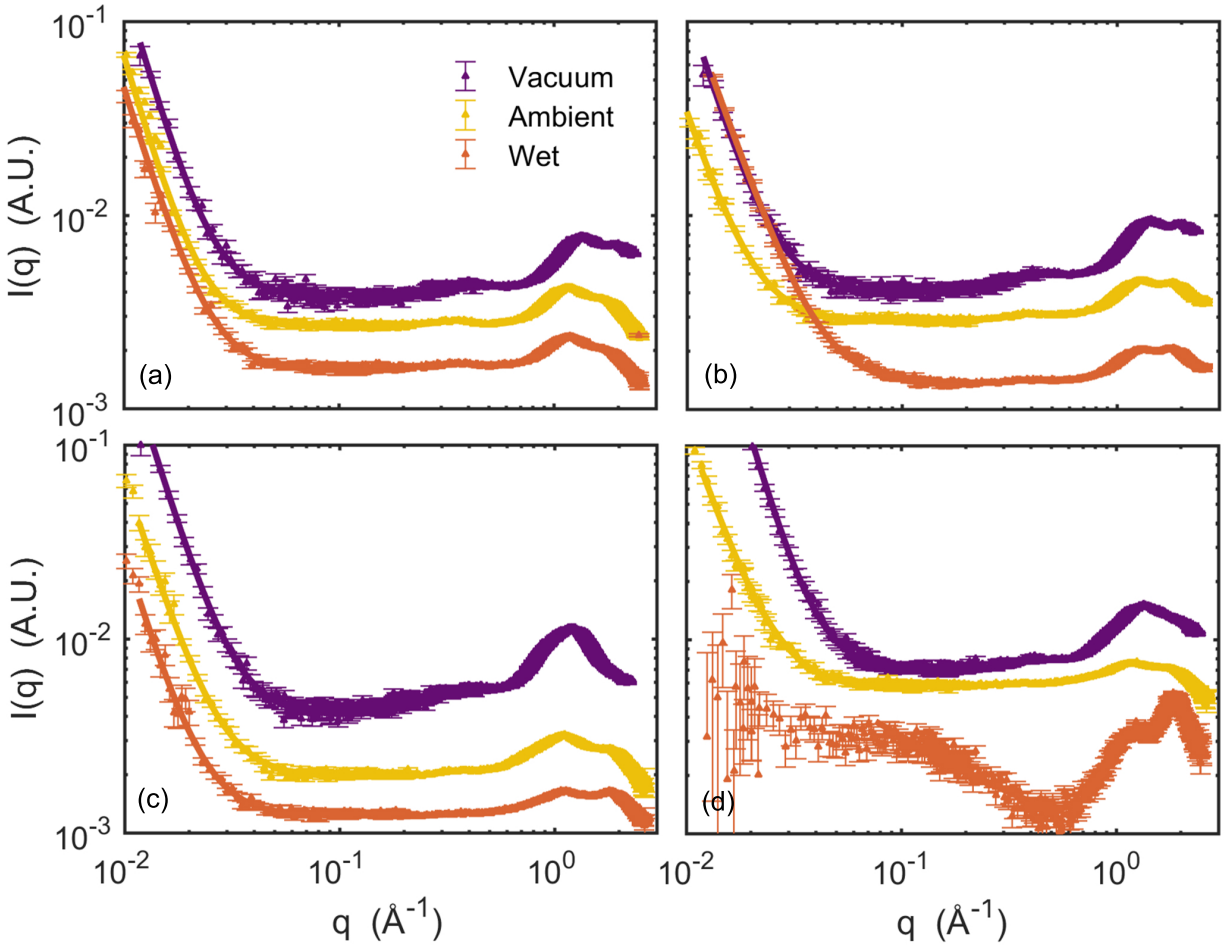

Figure 4: X-ray scattering profiles of films of (a) 80.2 and (b) 97.5% dm HMT-PMBI(I^-) and (c) 80.2% and (d) 97.5% dm HMT-PMBI(Cl^-) at various levels of hydration: in vacuum (purple), in ambient conditions (mustard), and fully hydrated (orange). In HMT-PMBI(Cl^-), Peak 2 significantly increases in intensity at ambient humidity and when hydrated. A vertical offset has been added to the data to reduce overlap.

The results of the two measurements were combined into the profiles shown in Figure 5 (b) by integrating 30° sections along the equatorial and meridional directions. In the stretched sample, Peak 0 is significantly stronger and narrower in the meridional as compared to equatorial sections while the intensity of Peak 1 is stronger in the equatorial as compared to the meridional sections. All peaks in the stretched sample are shifted to lower q than observed in the unstretched sample.

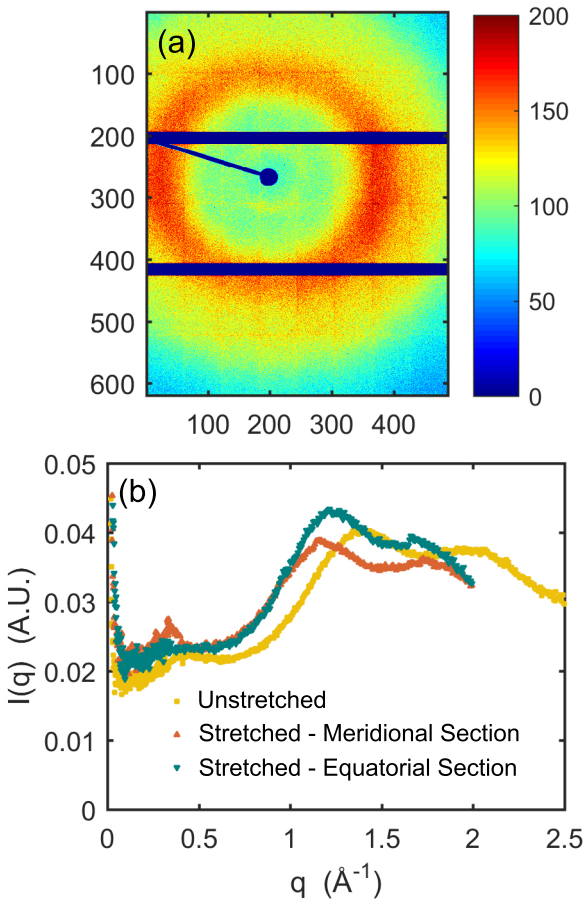

Figure 5: (a) Image from the 2-D detector and (b) integrated X-ray scattering from stretched and unstretched 89.7% dm HMT-PMBI(I^-). Data for the unstretched sample is shown in yellow. Data for the stretched sample from meridional and equatorial sections are shown in orange and green, respectively.

Discussion

In all of the results shown in Figures 3-5, the small-angle behavior is dominated by a low-q upturn; no structural features are visible in this q-range in any material, indicating that no phase separation is occurring on length scales longer than a couple of nanometers. Small-angle neutron scattering results (described in the Supporting Information) confirm this observation.

All of the ionenes show two prominent WAXS peaks. Peak 1 corresponds to a length scale of approximately 6 Å while Peak 2 corresponds to length scale of approximately 4 Å. Because Peak 1 becomes stronger in the equatorial direction after stretching, we associate it with a backbone-backbone correlation length. As the film is stretched, the molecules become straighter and more parallel, enhancing the scattering in the direction perpendicular to the stretching direction.[20] Furthermore, there is a change in peak position; the peak in the data from the equatorial section appears at approximately 1.2 $Å^{-1}$, 10% below the position of Peak 1 in the unstretched material. This is consistent with the difference in peak position between randomly oriented and parallel polymer chains with similar stacking lengths.[31]

We associate Peak 2 with the ion-backbone and water-backbone spacings because the intensity of Peak 2 is strongly correlated with both the degree of methylation and the water content of the material. Peak 2 dramatically increases in intensity and shifts to lower q when samples with greater degrees of methylation are hydrated, reflecting their large water uptake.

In the stretched material, the MAXS peak, Peak 0, is not visible in the equatorial section, and becomes more intense and shifts to lower q by approximately 25% (from 0.43 to 0.33 $Å^{-1}$) in the meridional section relative to the unstretched material. As the film is stretched and the polymer chains become more parallel, correlation between monomers should increase.[20] This suggests that Peak 0 corresponds to a length scale along the polymer backbone, presumably a monomer-monomer correlation length with some contribution from the associated anions. The length scale associated with Peak 0, approximately 20 Å,

is slightly lower than the observed, fully-extended monomer length in our DFT calculation, approximately 22 Å, highlighted in Fig. 2. In previous work, we observed a similar peak in an uncharged benzimidazole-based material, again at a length scale corresponding to the expected monomer length.[32] We expect that the shift in peak position to lower q is caused by some combination of orientation and straightening of the polymer chains. A shift of up to 22% could be explained by a length scale shifting from isotropic to fully ordered; this is the difference between the Debye and the Bragg lengths for amorphous and crystalline material, respectively.[31]

Fitting Eq. S1 to the data results in estimates for the length scales d_0, d_1, and d_2 associated with Peaks 0, 1 and 2. The results are shown in Figure 6. Parts (a) and (b) show the length scale associated with Peak 0, d_0, which we attribute to the monomer-monomer correlation length along the backbone. Parts (c) and (d) show the length scales associated with Peak 1, d_1, which we attribute to the inter-backbone spacing, and Peak 2, d_2, which we attribute to the ion-backbone spacing. Parts (a) and (c) compare I^- samples at various levels of hydration: in vacuum, in ambient conditions, and fully hydrated for samples of different charge content while Parts (b) and (d) compare results for the I^- and Cl^- forms in vacuum.

Methylation of the polymer impacts two of the three length scales. The monomer-monomer correlation length and backbone-backbone correlation length decrease with increasing methylation, with the effect being more noticeable in the case of d_0. Increased methylation results in the molecule becoming more charged, with accompanying counter ions. The additional methyl groups also place constraints on the molecular configurations. We postulate that the effect of increased constraints results in a decreased monomer-monomer length and the decreased flexibility and additional charge allows for slightly better packing. While the amplitude of Peak 2 (attributed to ion/water-backbone scattering) increases significantly with methylation, d_2 is independent of methylation.

Figures 6 (a) and (c) show that all three length scales are 10-12% larger in ambient

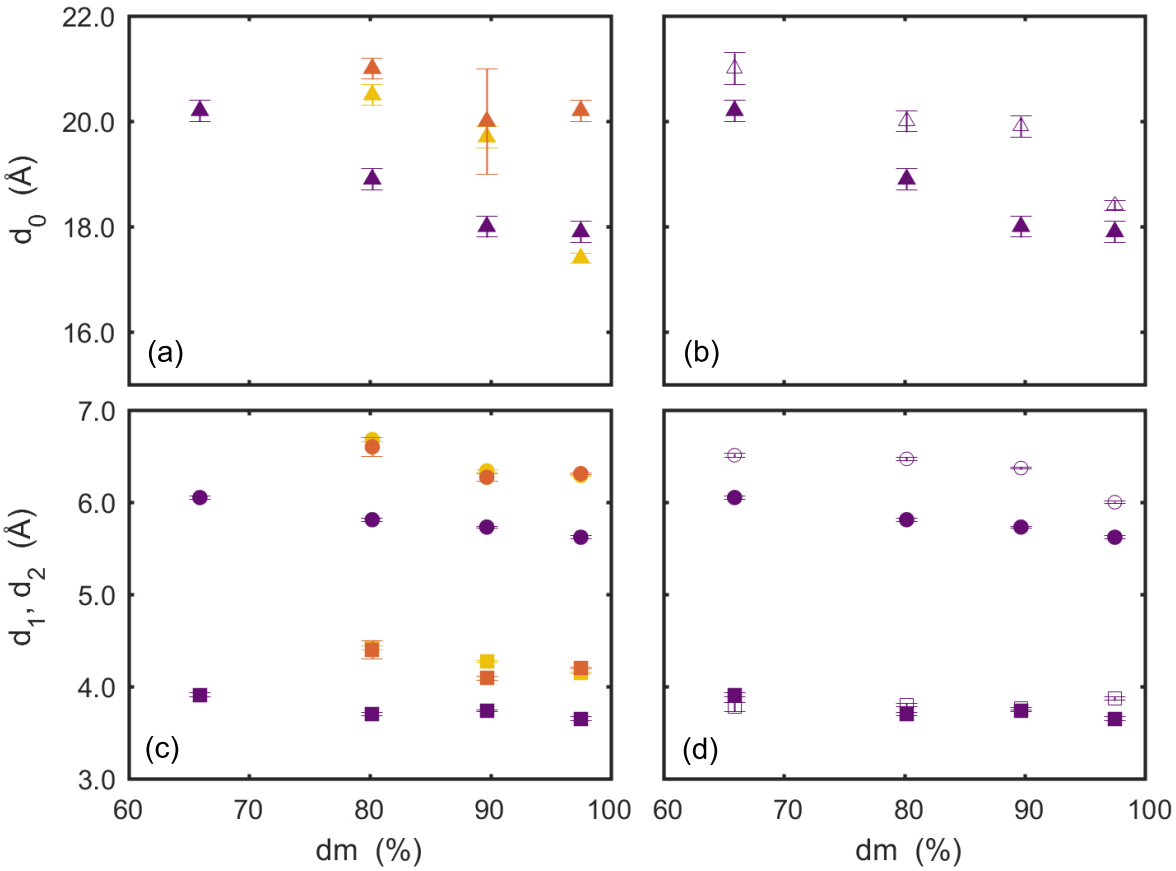

Figure 6: The length scales d_0, d_1, and d_2 associated with Peaks 0, 1 and 2 obtained by fitting Eq. SI 1 to the data. (a) Comparison of d_0 for I^- form at various levels of hydration: in vacuum (purple triangles), in ambient conditions (gold triangles), and fully hydrated (orange triangles). (b) Comparison of d_0 for I^- (closed triangles) and Cl^- (open triangles) forms. (c) Comparison of d_1 (circles)and d_2 (squares) for I^- form at various levels of hydration: in vacuum (purple symbols), in ambient conditions (gold symbols), and fully hydrated (orange symbols). (d) Comparison of d_1 (circles) and d_2 (squares) for I^- (closed symbols) and Cl^- (open symbols) forms. The error bars are the uncertainties in the fit parameters.

conditions relative to vacuum, however the difference between these length scales in ambient and fully-hydrated samples are negligible. This is consistent with swelling occurring in the presence of water. Hydration leads to larger monomer-monomer distances, backbone-backbone distances, and ion-backbone distances. The change in morphology at the nanoscale is consistent with dimensional measurements of 89.7% HMT-PMBI(I^-) which demonstrate a 30% increase in volume and a 10% increase in directional swelling.[17]

The monomer-monomer and backbone-backbone lengths depend on the anion, as shown in Figures 6 (b) and (d). The monomer-monomer length d_0 is 5% larger in Cl^- than I^- form while d_1 is 10% larger in Cl^- than I^- form. The smaller anion may allow the polymer backbone more freedom to elongate. These observations suggest that the anion-backbone distance is independent of charge content, and roughly the same in Cl^- and I^- forms.

The measurement of wet 97.5% dm HMT-PMBI(Cl^-) shows a mid-q shoulder (Fig. 4d). To associate a length scale with this feature, we fit the Correlation Length Model, Eq. S2 to this region of the data resulting in a correlation length of 4.3 ± 0.3 Å. This feature is not present in any of the other samples, or this sample at lower levels of hydration. This sample contains substantially more water than the others (Table 1); this appears to be the first indication of larger water-rich regions.

To confirm our interpretation of the scattering results, we performed molecular dynamics simulations using the NAnonscale Molecular Dynamics (NAMD) package for a fully-methylated sample consisting of 25 tetramers. We compared results for 6 and 18 water molecules per monomer. Three water molecules per iodide ion ($\lambda = 3$) was chosen to represent material in ambient conditions, while 9 water molecules per iodide ($\lambda = 9$) was selected to represent the fully hydrated membrane. The equilibrated cell for $\lambda = 3$ had a density of 1.37 g/ml, while the cell for $\lambda = 9$ had a density of 1.35 g/ml, similar to the approximately 1.3 g/ml density of pristine PBI.

The results of our molecular dynamics simulation are shown in Figure 7. Figures 7(a) and (b) show the cell at the conclusion of the simulation; Fig. 7(a) shows results for a cell

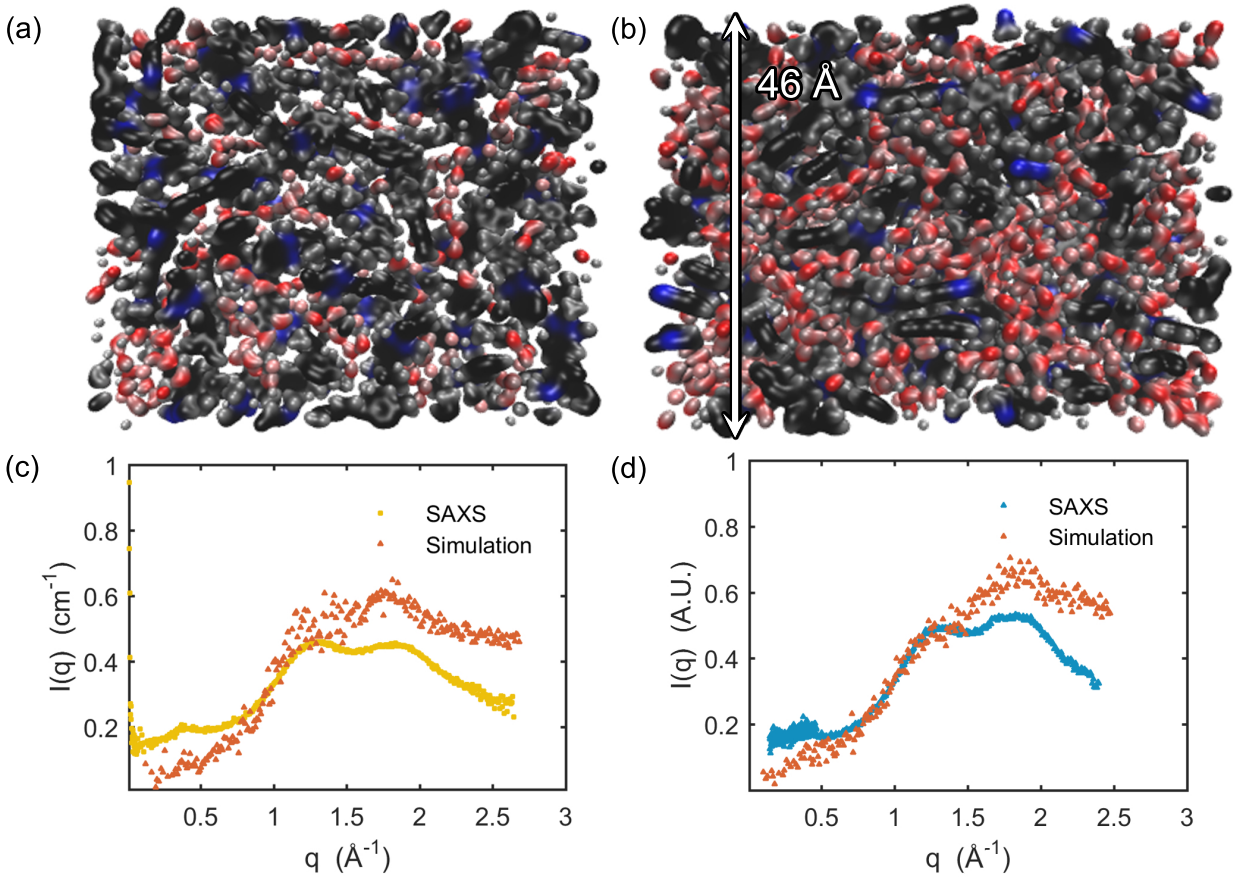

Figure 7: The results of the molecular dynamics simulation for a cell containing 25 100% dm tetramers for (a) 600 water molecules, corresponding to λ=3, and (b) 1800 water molecules, corresponding to λ=9. The colours represent carbon (black), nitrogen (blue), hydrogen (grey), oxygen (red), and iodide (pink). The structures correspond to surfaces of constant electron density. Parts (c) and (d) compare the structure factor calculated from the simulation data (orange) to the observed X-ray scattering profile for 97.5% dm HMT-PMBI(I^-) under (c) ambient conditions, λ=3, (yellow) and (d) hydrated, λ=9, (blue). The λ=9 cell is approximately 46 Å tall, as indicated by the white arrow in part (b).

at $\lambda = 3$, and Fig. 7(b) shows results for a cell at $\lambda = 9$. The figures are estimated electron density isosurfaces produced by the VMD QuickSurf representation:[33] (black), nitrogen (blue), hydrogen (grey), oxygen (red), and iodide (pink). The polymer chains, shown as blue, black and grey isosurfaces, appear to be randomly oriented, and as in the scattering data, no long-range order is visible. The water molecules, shown as red and grey isosurfaces, appear to form a network connecting the anions, shown in pink, and the cationic sites to each other. Remarkably, the distance between the backbones is similar in the two cells; the water forms strands in the $\lambda = 3$ cell, while it fills all of the empty space in the $\lambda = 9$ cell but, in either case, a network is formed. The percolating network, and lack of discrete ion clusters, is similar to what was observed by Frischknecht et al. in coarse-grained simulations of model ionenes.[34,35] In that research, ionenes were found to readily form percolating networks while pendant ionomers tended to be characterized by the presence of ionic aggregates.

Figures 7(c) and (d) compare the structure factor of the (c) $\lambda = 3$ and (d) $\lambda = 9$ simulation cells to the experimentally observed X-ray scattering profiles of 97.5% dm HMT-PMBI(I^-) under ambient and wet conditions, where it has similar water contents. The three peaks observed in the scattering profiles are reproduced by the simulation. While the relative intensities of the peaks are different, this is an expected consequence of neglecting the form factors of the atoms. Several individual correlation functions were also calculated from the data; these are included in the Supplemental Information as Fig. S3. Examination of the correlation functions confirms our interpretation of Peaks 0, 1 and 2.

The ability of the polymer to form a network of hydrophilic pores is an important feature of the conductivity of these materials, which is higher than expected for a truly random polymer system. A polymer such as HMT-PMBI that becomes glassy during solution casting will not necessarily collapse to the optimal packing, and some space will be left behind, as is reported in polyimide materials.[36] This affect may be enhanced by casting in iodide form, as iodide is a particularly bulky ion. In fact, films cast from polymer in the iodide form uptake significantly less water than they do after exchange with other ions.[17]

Conclusions

We have investigated the morphology of a novel series of anion-conducting polymers, HMT-PMBI, with degrees of methylation ranging from 65.9% to 97.5%. Our studies included X-ray and neutron scattering, supplemented by gas-phase density functional theory calculations for the series and molecular dynamics simulations of a twenty-five tetramer cell for the fully-methylated form. Length scales associated with the intramolecular monomer-monomer spacing, backbone-backbone, and ion-backbone spacings were identified in the scattering data, and were consistent with simulation results. This represents the first structural investigation of these promising materials.

The small peak at mid-scattering angles, labeled Peak 0, has been assigned to an intramolecular monomer-monomer spacing. In HMT-PMBI(I^-) samples, the peak corresponds to a length scale of 17.6 Å to 20.4 Å, and slightly higher for chloride-form materials. The value for 97.5% dm in the iodide form is similar to the result calculated for the length of the central monomer in the gas-phase DFT calculation, 22 Å. These calculations, where the monomers are in vacuum, are performed on fully methylated HMT-PMBI, shown in Figure 2. This interpretation is strengthened by the effect of stretching on the 89.7% dm HMT-PMBI(I^-) sample, as this peak is suppressed in the equatorial direction and both sharpened and shifted from 0.43 $Å^{-1}$ to approximately 0.33 $Å^{-1}$ in the meridional direction. The effect of stretching the polymer is analogous to combing: it is expected that the chains would be straightened and preferably oriented in the direction parallel to the stretching.

We have assigned the WAXS peaks to angstrom-scale correlations between adjacent polymer chains, ions, and water molecules. We conclude that the highest-q peak (Peak 2) corresponds to correlation between the backbones, halogens, and water. This is supported by a number of factors, the most obvious being that it increases in strength with IEC, and both increases in strength and shifts to lower q when the material is hydrated. A similar length scale is shown in the molecular dynamics simulation, where the iodide-oxygen and oxygen-oxygen spacings are shown to be shorter than the iodide-carbon length scale. We

have assigned the first WAXS peak (Peak 1) to both packing between backbone atoms in adjacent chains, and correlation between ion-water channels. These features are visible at the ~ 6 Å length scale in the simulation, and it is common in the literature to assign the first clear WAXS peak to interchain stacking in polymers.[31] Furthermore, it strengthens relative to the higher-q peak as the degree of methylation is lowered. This interpretation is also strengthened by the effect of stretching on the WAXS profile; the peak shifted to lower q in the stretched material and sharpened in the equatorial direction.

Samples containing a moderate amount of water ($<$40%) showed no other features in their scattering profiles. When fully hydrated, the 97.5% dm HMT-PMBI(Cl^-) showed structure corresponding to a correlation length of 4.3 Å. These results show that, even when hydrated, these materials contain no phase separation or water clustering on length scales greater than six angstroms and no characteristic length scales at all above the monomer length. This is uncommon among high-performance fuel cell membranes. MD simulations indicate that the water and ions in the membrane form an inter-penetrating network where conductivity can occur.

Acknowledgement

Financial support for this study was provided by Natural Sciences and Engineering Research Council of Canada (NSERC). Research described in this work made use of the 4D LABS shared facilities at SFU supported by the Canada Foundation for Innovation (CFI), British Columbia Knowledge Development Fund (BCKDF), Western Economic Diversification Canada (WD), and Simon Fraser University (SFU). Neutron scattering experiments were performed at the Labratoire Léon Brillouin (Saclay, France) by Dr. Sandrine Lyonnard. Water uptake measurements were performed by Jonathon Ward at Simon Fraser University. This research was enabled in part by support provided by WestGrid (www.westgrid.ca) and Compute Canada Calcul Canada (www.computecanada.ca).

Supporting Information Available

The Supplementary Information file includes the following:

- Details of simulations;
- Neutron scattering results;
- Detailed description of analysis of X-ray scattering data; and
- Parameters obtained by fitting the model function to the X-ray scattering data;

References

(1) Marini, S.; Salvi, P.; Nelli, P.; Pesenti, R.; Villa, M.; Berrettoni, M.; Zangari, G.; Kiros, Y. Advanced Alkaline Water Electrolysis. *Electrochim. Acta* **2012**, *82*, 384–391.

(2) Krol, J.; Wessling, M.; Strathmann, H. Concentration Polarization with Monopolar Ion Exchange Membranes: Current–Voltage Curves and Water Dissociation. *J. Membr. Sci.* **1999**, *162*, 145–154.

(3) Kreuer, K.-D. Ion Conducting Membranes for Fuel Cells and Other Electrochemical Devices. *Chem. Mater.* **2013**, *26*, 361–380.

(4) Gellett, W.; Schumacher, J.; Kesmez, M.; Le, D.; Minteer, S. D. High Current Density Air-Breathing Laccase Biocathode. *J. Electrochem. Soc.* **2010**, *157*, B557–B562.

(5) Varcoe, J. R.; Atanassov, P.; Dekel, D. R.; Herring, A. M.; Hickner, M. A.; Kohl, P. A.; Kucernak, A. R.; Mustain, W. E.; Nijmeijer, K.; Scott, K. et al. Anion-Exchange Membranes in Electrochemical Energy Systems. *Energy Environ. Sci.* **2014**, *7*, 3135–3191.

(6) Pan, J.; Chen, C.; Zhuang, L.; Lu, J. Designing Advanced Alkaline Polymer Electrolytes for Fuel Cell Applications. *Acc. Chem. Res.* **2011**, *45*, 473–481.

(7) Neagu, V.; Bunia, I.; Plesca, I. Ionic Polymers VI. Chemical Stability of Strong Base Anion Exchangers in Aggressive Media. *Polym. Degrad. Stab.* **2000**, *70*, 463–468.

(8) Dekel, D. R. Review of Cell Performance in Anion Exchange Membrane Fuel Cells. *J. Power Sources,* in press.

(9) Zhang, Q.; Li, S.; Zhang, S. A Novel Guanidinium Grafted Poly (Aryl Ether Sulfone) for High-Performance Hydroxide Exchange Membranes. *Chem. Commun.* **2010**, *46*, 7495–7497.

(10) Faraj, M.; Elia, E.; Boccia, M.; Filpi, A.; Pucci, A.; Ciardelli, F. New Anion Conducting Membranes Based on Functionalized Styrene–Butadiene–Styrene Triblock Copolymer for Fuel Cells Applications. *J. Polym. Sci., Part A: Polym. Chem.* **2011**, *49*, 3437–3447.

(11) Guo, M.; Fang, J.; Xu, H.; Li, W.; Lu, X.; Lan, C.; Li, K. Synthesis and Characterization of Novel Anion Exchange Membranes Based on Imidazolium-Type Ionic Liquid for Alkaline Fuel Cells. *J. Membr. Sci.* **2010**, *362*, 97–104.

(12) Gu, F.; Dong, H.; Li, Y.; Sun, Z.; Yan, F. Base Stable Pyrrolidinium Cations for Alkaline Anion Exchange Membrane Applications. *Macromolecules* **2014**, *47*, 6740–6747.

(13) Zhang, B.; Gu, S.; Wang, J.; Liu, Y.; Herring, A. M.; Yan, Y. Tertiary Sulfonium as a Cationic Functional Group for Hydroxide Exchange Membranes. *RSC Adv.* **2012**, *2*, 12683–12685.

(14) Gu, S.; Cai, R.; Luo, T.; Chen, Z.; Sun, M.; Liu, Y.; He, G.; Yan, Y. A Soluble and Highly Conductive Ionomer for High-Performance Hydroxide Exchange Membrane Fuel Cells. *Angew. Chem., Int. Ed.* **2009**, *48*, 6499–6502.

(15) Zha, Y.; Disabb-Miller, M. L.; Johnson, Z. D.; Hickner, M. A.; Tew, G. N. Metal-Cation-Based Anion Exchange Membranes. *J. Am. Chem. Soc.* **2012**, *134*, 4493–4496.

(16) Wright, A. G.; Holdcroft, S. Hydroxide-Stable Ionenes. *ACS Macro Lett.* **2014**, *3*, 444–447.

(17) Wright, A. G.; Fan, J.; Britton, B.; Weissbach, T.; Lee, H.-F.; Kitching, E. A.; Peckham, T. J.; Holdcroft, S. Hexamethyl-p-Terphenyl Poly (Benzimidazolium): a Universal Hydroxide-Conducting Polymer for Energy Conversion Devices. *Energy Environ. Sci.* **2016**, *9*, 2130–2142.

(18) Wright, A. G.; Weissbach, T.; Holdcroft, S. Poly (Phenylene) and m-Terphenyl as Powerful Protecting Groups for the Preparation of Stable Organic Hydroxides. *Angew. Chem., Int. Ed.* **2016**, *55*, 4818–4821.

(19) Shin, D. W.; Guiver, M. D.; Lee, Y. M. Hydrocarbon-Based Polymer Electrolyte Membranes: Importance of Morphology on Ion Transport and Membrane Stability. *Chem. Rev.* **2017**, *117*, 4759–4805.

(20) Roe, R.-J. *Methods of X-Ray and Neutron Scattering in Polymer Science*; Oxford University Press, 2000.

(21) Frisch, M. J.; et al., *Gaussian 09, Revision D*; Gaussian, Inc, 2009.

(22) Becke, A. D. A New Mixing of Hartree–Fock and Local Density-Functional Theories. *J. Chem. Phys.* **1993**, *98*, 1372–1377.

(23) Schäfer, A.; Horn, H.; Ahlrichs, R. Fully Optimized Contracted Gaussian Basis Sets for Atoms Li to Kr. *J. Chem. Phys.* **1992**, *97*, 2571–2577.

(24) Henkensmeier, D.; Cho, H.; Brela, M.; Michalak, A.; Dyck, A.; Germer, W.; Duong, N. M. H.; Jang, J. H.; Kim, H.-J.; Woo, N.-S. et al. Anion Conducting Polymers Based on Ether Linked Polybenzimidazole (PBI-OO). *Int. J. of Hydrogen Energy* **2014**, *39*, 2842–2853.

(25) McDermott, A. G.; Larsen, G. S.; Budd, P. M.; Colina, C. M.; Runt, J. Structural Characterization of a Polymer of Intrinsic Microporosity: X-ray Scattering with Interpretation Enhanced by Molecular Dynamics Simulations. *Macromolecules* **2011**, *44*, 14–16.

(26) Perry, K. A.; More, K. L.; Payzant, A. E.; Meisner, R. A.; Sumpter, B. G.; Benicewicz, B. C. A Comparative Study of Phosphoric Acid-Doped m-PBI Membranes. *J. Polym. Sci., Part B: Polym. Phys.* **2014**, *52*, 26–35.

(27) Phillips, J. C.; Braun, R.; Wang, W.; Gumbart, J.; Tajkhorshid, E.; Villa, E.; Chipot, C.; Skeel, R. D.; Kale, L.; Schulten, K. Scalable Molecular Dynamics with NAMD. *J. Comput. Chem.* **2005**, *26*, 1781–1802.

(28) Kalé, L.; Skeel, R.; Bhandarkar, M.; Brunner, R.; Gursoy, A.; Krawetz, N.; Phillips, J.; Shinozaki, A.; Varadarajan, K.; Schulten, K. NAMD2: Greater Scalability for Parallel Molecular Dynamics. *J. Comput. Phys.* **1999**, *151*, 283–312.

(29) Jorgensen, W. L.; Maxwell, D. S.; Tirado-Rives, J. Development and Testing of the OPLS All-Atom Force Field on Conformational Energetics and Properties of Organic Liquids. *J. Am. Chem. Soc.* **1996**, *118*, 11225–11236.

(30) Vanommeslaeghe, K.; Hatcher, E.; Acharya, C.; Kundu, S.; Zhong, S.; Shim, J.; Darian, E.; Guvench, O.; Lopes, P.; Vorobyov, I. et al. CHARMM General Force Field: A force field for drug-like molecules compatible with the CHARMM all-atom additive biological force fields. *JJ. Comput. Chem.* **2010**, *31*, 671–690.

(31) Alexander, L. E. *X-ray Diffraction Methods in Polymer Science*; John Wiley & Sons, Inc., 1969.

(32) Schibli, E. M. Analysis of Novel Ionenes via X-ray and Neutron Scattering. M.Sc. thesis, Simon Fraser University, 2016.

(33) Krone, M.; Stone, J.; Ertl, T.; Schulten, K. Fast Visualization of Gaussian Density Surfaces for Molecular Dynamics and Particle System Trajectories. EuroVis - Short Papers. 2012; pp 67–71.

(34) Hall, L. M.; Stevens, M. J.; Frischknecht, A. L. Effect of Polymer Architecture and Ionic Aggregation on the Scattering Peak in Model Ionomers. *Phys. Rev. Lett.* **2011**, *106*, 127801.

(35) Hall, L. M.; Seitz, M. E.; Winey, K. I.; Opper, K. L.; Wagener, K. B.; Stevens, M. J.; Frischknecht, A. L. Ionic Aggregate Structure in Ionomer Melts: Effect of Molecular Architecture on Aggregates and the Ionomer Peak. *J. Am. Chem. Soc.* **2012**, *134*, 574–587, PMID: 22133577.

(36) Marestin, C.; Gebel, G.; Diat, O.; Mercier, R. Sufonated Polyimides. *Adv. Polym. Sci.* **2008**, *216*, 185–258.

Graphical TOC Entry